PROCEEDINGS OF SCIENCE

Electroweak penguins with di-leptons at LHCb

Michal Kreps[*†]
University of Warwick
E-mail: M.Kreps@warwick.ac.uk

The studies of angular distributions and differential branching fractions of the decays $B^0 \to K^{*0}\mu^+\mu^-$ and $B_s^0 \to \phi\mu^+\mu^-$ are presented. They are complemented by the evidence of the $B^0 \to K^{*0}e^+e^-$ decay for events with the e^+e^- invariant mass between 30 and 1000 MeV/c. The presented results are based on the data sample collected by the LHCb experiment, which corresponds to an integrated luminosity of 1.0 fb^{-1}. Where predictions exist, all obtained result are consistent with the Standard Model and put strong constraints on the $b \to s$ flavour changing neutral current processes.

14th International Conference on B-Physics at Hadron Machines,
April 8-12, 2013
Bologna, Italy

[*]Speaker.
[†]On behalf of the LHCb collaboration.

PoS(Beauty 2013)031

1. Introduction

The rare flavour changing neutral current decays of B-hadrons governed by the $b \to s$ quark level transition provide an excellent probe for physics beyond the Standard Model (SM). In the SM these decays are forbidden at the tree level and proceed through loop level box and penguin diagrams shown in Fig. 1. The final states which contain a pair of leptons together with a single hadron is especially interesting as it simplifies theoretical predictions and thus improves prospects in searches for a physics beyond SM. An angular analysis of the decay allows several observables to be constructed, which are largely free from form factor uncertainties and allow precise tests of the SM.

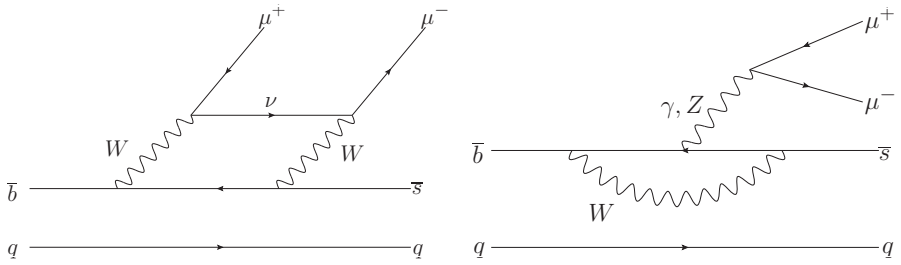

Figure 1: Dominant SM Feynman diagrams for decays of B^0 ($q = d$) and B_s^0 ($q = s$) mesons into a light meson and a pair of muons.

The theory prediction within SM for the $B^0 \to K^{*0}\mu^+\mu^-$ decay used in these proceedings is described in Ref. [1]. Depending on the q^2 region different approaches are used. At the low q^2, the prediction is based on QCD factorization and soft collinear effective theory [2]. For the high q^2 region an operator product expansion in inverse b-quark mass and $1/\sqrt{q^2}$ is employed to estimate the long-distance contributions [3, 4]. The form factors used are provided by Ref. [5]. For the B_s^0 decay prediction shown later is provided by Ref. [6] with the form factors from the same source as for the B^0 decay [5]. In this prediction, the B_s^0 mixing is incorporated as described in Ref. [7].

In these proceedings we will review latest LHCb results on $B^0 \to K^{*0}\mu^+\mu^-$ [8], $B_s^0 \to \phi\mu+\mu^-$ [9] and $B^0 \to K^{*0}e^+e^-$ [10] decays. All results are based on data collected in 2011 at $\sqrt{s} = 7$ TeV, with corresponding integrated luminosity of 1 fb^{-1}.

2. Data selection

In the three measurements presented, the candidate selection follows same steps. It starts from a relatively loose selection to reduce the number of candidates to a manageable level. This is followed by the boosted decision tree which combines kinematic, topological and particle identification inputs into a single quantity on which a final requirement is imposed. The background training sample is composed of the candidates with invariant masses above the B (B_s^0) meson mass. For the signal, background subtracted data or samples of simulated events are used, depending on the available statistics. The reconstructed final state contains not only decays of interest, but also decays through charmonium resonances, where the charmonium resonance decays to two leptons. As the branching fraction for those is much higher than for the semileptonic $b \to sl^+l^-$ decays,

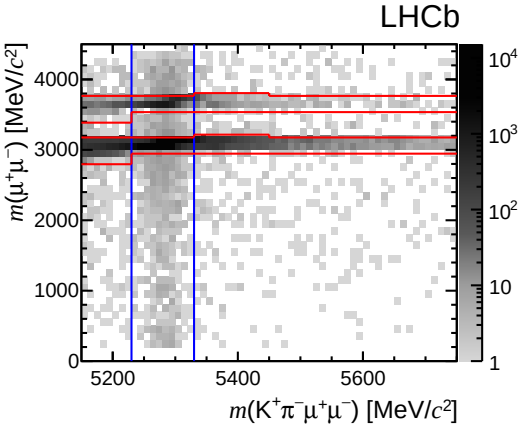

Figure 2: The distribution of $B^0 \to K^{*0}\mu^+\mu^-$ candidates in the $m(\mu^+\mu^-)$-$m(K^+\pi^-\mu^+\mu^-)$ plane. The region between vertical lines indicates the B^0 signal region, while the two sets of horizontal lines indicate J/ψ and $\psi(2S)$ regions which are removed from the analysis.

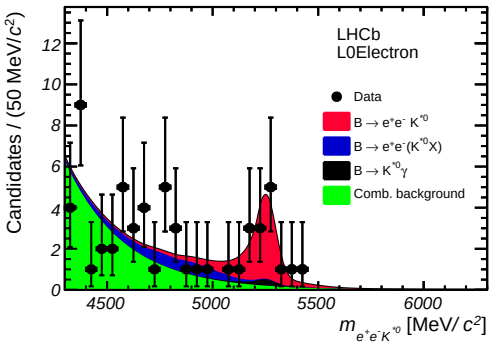

Figure 3: The invariant mass distribution of $B^0 \to K^{*0}e^+e^-$ candidates with dimuon invariant mass between 30 and 1000 MeV/c^2. Only part of the data selected by one of the trigger selection is shown.

those will dominate in the corresponding regions. As example, in Fig. 2 we show $B^0 \to K^{*0}\mu^+\mu^-$ candidates in the $m(\mu^+\mu^-)$-$m(K^+\pi^-\mu^+\mu^-)$ plane, where m denotes invariant mass of given set of particles. The charmonium resonances veto is rather complicated as indicated in Fig. 2. The shape of the veto is driven by the desire to remove decays through charmonia where a photon is radiated or which are misreconstructed as much as possible. This approach complicates the extraction of the yields for the differential branching fraction, but at the same time it simplifies the treatment of background in the angular distributions fit. For the differential branching fraction measurements, the decays proceeding via J/ψ resonance are used for normalization. As they are reconstructed in the same final state, most systematic effects cancel out.

3. Differential branching fraction

From the experimental point of view, the measurement of the differential branching fraction as a function of q^2 is one of the easiest. While its sensitivity to physics beyond SM is reduced due to the relatively large uncertainties on the form factors, it is still useful probe.We split data into six q^2 intervals and in each interval the differential branching fraction is estimated as

$$\frac{\mathrm{d}\mathscr{B}}{\mathrm{d}q^2} = \frac{1}{\Delta q^2}\frac{N_{\mathrm{sig}}}{N_{\mathrm{norm}}}\varepsilon_{\mathrm{rel}}\mathscr{B}(H_b \to J/\psi h)\mathscr{B}(J/\psi \to \mu^+\mu^-), \tag{3.1}$$

where the N_{sig} and N_{norm} are yields of the rare and the normalization decays, the $\varepsilon_{\mathrm{rel}}$ is relative efficiency between two channels and the Δq^2 denotes width of the q^2 interval. The H_b denotes B^0 or B_s^0 while h is corresponding light hadron. Over the full q^2 range we observe 883 ± 34 $B^0 \to K^{*0}\mu^+\mu^-$ and 174 ± 15 $B_s^0 \to \phi\mu^+\mu^-$ signal decays in the rare decay with non-resonant muon pair. The measured differential branching fractions are shown in Fig. 4. The measurement effectively

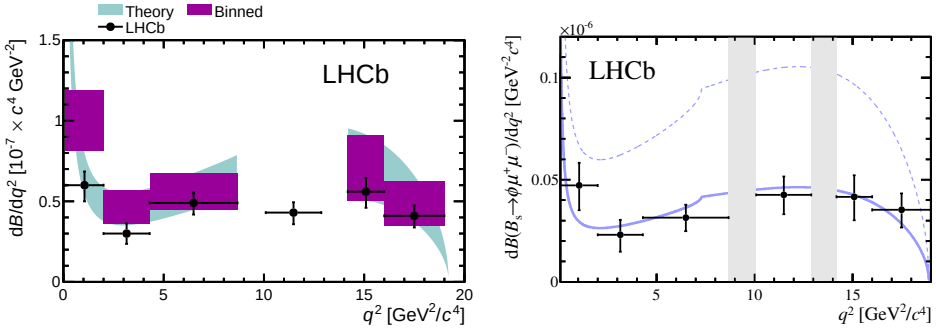

Figure 4: The differential branching fraction as a function of q^2 for the $B^0 \to K^{*0}\mu^+\mu^-$ (left) and the $B^0_s \to \phi\mu^+\mu^-$ (right) decays. The shaded regions on the right-hand plot show regions removed due to the presence of decays through the charmonium resonances. The blue curve in the righ-hand plot shows SM prediction normalized to two different total branching fractions. The light shaded area in the left-hand plot indicates the SM prediction with its uncertainty. The dark area is the average of the SM prediction over the q^2 interval.

represents an average over the q^2 interval. In both B^0 and B^0_s decays the observed shape of the differential branching fraction agrees with SM expectation.

The low q^2 region is particularly sensitive to the photon polarization. In order to reach as low q^2 values as possible, we investigate also the decay $B^0 \to K^{*0}e^+e^-$. We reconstruct events with the e^+e^- pair invariant mass between 30 and 1000 MeV/c^2. The lower limit is driven by the fact that below 30 MeV/c^2 we cannot experimentally define the dilepton decay plane and thus below this limit we cannot perform the angular analysis. In the selected q^2 region we observe about 30 $B^0 \to K^{*0}e^+e^-$ signal decays. The invariant mass distribution of a subset of the candidates, where the event was triggered in the hardware trigger by one of the particles from the B^0 decay, is shown in Fig. 3. The observed signal has a significance of 4.6 standard deviations and corresponds to a branching fraction of $(3.1\,^{+0.8}_{-0.8}\,^{+0.2}_{-0.3} \pm 0.2) \times 10^{-7}$.

4. Angular analysis formalism

In order to achieve the best sensitivity to physics beyond SM, an angular analysis is required. For the fit to data, the sum of the differential decay width for B^0 and $\bar{B}^0$ is used with the assumption of equal production rate for B^0 and $\bar{B}^0$ mesons. With the assumption that $q^2 >> 4m^2_\mu$ and transformation of the angle between $\mu^+\mu^-$ and $K^+\pi^-$ planes to range between 0 and π (for details see Ref. [8]), the angular distribution for the $B^0 \to K^{*0}\mu^+\mu^-$ decay has the form

$$\begin{aligned}\frac{1}{d\Gamma/dq^2}\frac{d^4\Gamma}{dq^2 d\Omega} = {} & F_L \cos^2\theta_K + \frac{3}{4}(1-F_L)(1-\cos^2\theta_K) \;\; - F_L\cos^2\theta_K(2\cos^2\theta_\ell - 1) \;\; + \\ & \frac{1}{4}(1-F_L)(1-\cos^2\theta_K)(2\cos^2\theta_\ell - 1) \;\; + \;\; S_3(1-\cos^2\theta_K)(1-\cos^2\theta_\ell)\cos 2\hat{\phi} \;\; + \\ & \frac{4}{3}A_{FB}(1-\cos^2\theta_K)\cos\theta_\ell \;\; + \;\; A_9(1-\cos^2\theta_K)(1-\cos^2\theta_\ell)\sin 2\hat{\phi}\;, \end{aligned} \tag{4.1}$$

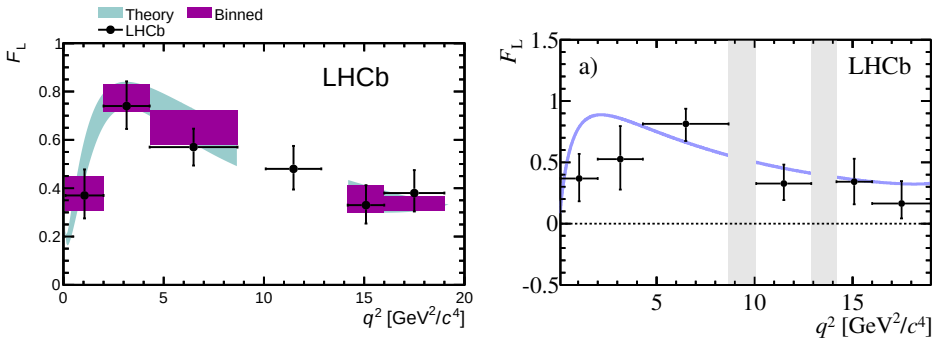

Figure 5: The fraction of longitudinal polarization of the K^{*0} (left) and the ϕ (right) mesons in corresponding decays. The points with error bars show the experimental results while the light shaded area in the left-hand plot and blue curve in the right-hand plot indicate the SM predictions. The dark area is the average of the theory prediction over the q^2 interval.

where the $\Omega = (\theta_l, \theta_K, \phi)$ denotes three angles describing decay in the helicity formalism. The F_L, A_{FB}, S_3 and A_9 observables can be expressed in terms of polarization amplitudes. The distribution for the $B_s^0 \to \phi\mu^+\mu^-$ decay follows similar ideas, and just differs by the fact that the analysed B_s^0 decay is not self-tagging. The details of the distribution are given in Ref. [9], with the main difference that without flavour tagging, the B_s^0 decay is not sensitive to the forward-backward asymmetry A_{FB} and is sensitive to the asymmetry between B_s^0 and $\bar{B}_s^0$ in the real part of the transverse amplitudes interference.

While the data sample available at LHCb is the largest from all experiments, it is not sufficient to be free of any potential statistical pitfalls. In the case of the B^0 decay, the observables themselves have to satisfy several boundary conditions. This makes the estimation of the statistical uncertainties difficult and thus the Feldman-Cousins method [**?**, 12] is employed to determine the 68% confidence intervals. In addition for the B_s^0 decay, due to the limited statistics available, the three projections are fitted consecutively to extract the observables. Again as in the case of the B^0 decay, also for the B_s^0 decay the Feldman-Cousins technique is employed to obtain the confidence intervals. While the confidence intervals guarantee coverage, it is difficult to provide correlations amongst observables.

5. Results of the angular analysis

Several observables are extracted from the angular analysis. The angular analysis of the $B_s^0 \to \phi\mu^+\mu^-$ decay is the first ever performed. As the first observable, in Fig. 5 we show the fraction of longitudinally polarized vector meson (K^{*0} or ϕ), F_L, as a function of q^2. The theory prediction for F_L is affected by form factors uncertainties and thus its sensitivity to physics beyond SM is decreased. Within the limited statistics of the B_s^0 sample, we observe a similar trend in the q^2 dependence of F_L as for the B^0 decay.

The second traditional observable from the angular analysis is the forward-backward asymmetry A_{FB}. The early measurements have indicated a possibility of disagreement with the theory predictions, but precision was not sufficient for a firm conclusion. As we do not perform flavour

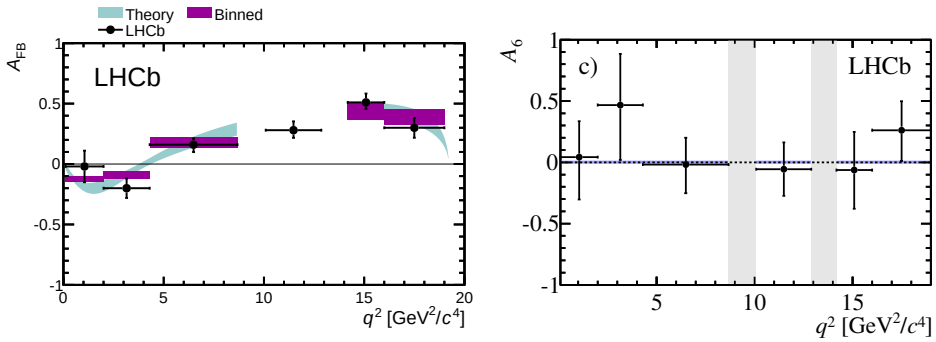

Figure 6: The forward-backward asymmetry for the $B^0 \to K^{*0}\mu^+\mu^-$ decay (left) and the asymmetry between B^0_s and $\bar{B}^0_s$ for the real part of the transverse amplitudes interference in the $B^0_s \to \phi\mu^+\mu^-$ decay (right).

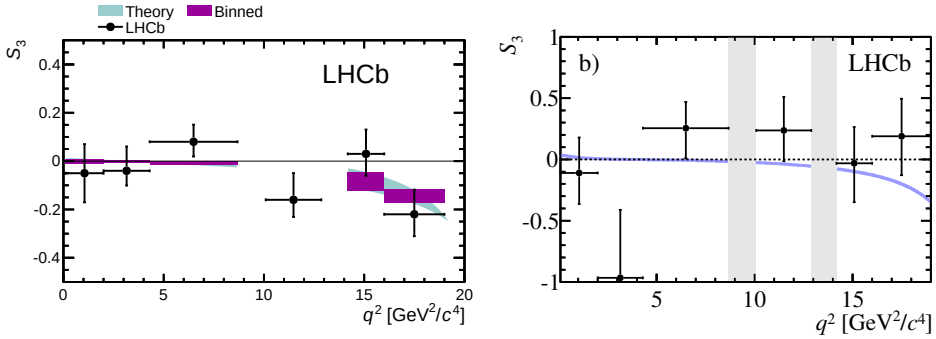

Figure 7: The asymmetry between the two transverse amplitudes averaged over $B^0_{(s)}$ and $\bar{B}^0_{(s)}$ for the B^0 (left) and the B^0_s (right) decays.

tagging for the B^0_s mesons, this observable is accessible only for the B^0 decays and it is shown in Fig. 6. While the theory prediction is affected by the form factor uncertainties, a q^2 point where A_{FB} crosses zero is rather well predicted. The LHCb experiment has measured this quantity for the first time. The measured value of (4.9 ± 0.9) GeV$^2/c^4$ is consistent with SM expectation.

Besides the well known F_L and A_{FB} observables, we measure several new observables. The first of these is the asymmetry between B^0_s and $\bar{B}^0_s$ for the real part of the transverse amplitudes interference, to which we have currently access only in the B^0_s decay. The result is consistent with zero across all q^2 intervals and shown in Fig. 6. The next observable is the asymmetry between the two transverse amplitudes averaged over $B^0_{(s)}$ and $\bar{B}^0_{(s)}$. It is expected to be close to zero over most of the q^2 intervals with a modest deviation from the zero at large q^2, close to the kinematical limit. The obtained results are shown in Fig. 7. Finally we come to the T-odd asymmetry from the interference of the two transverse amplitudes, A_9. This observable provides sensitivity to CP-violating effects through the CPT theorem when strong phases are close to zero and thus CP violation is not experimentally observable. The observable A_9 is specially sensitive to the right handed currents. The results from our measurements, for both B^0 and B^0_s decays, are shown in Fig. 8.

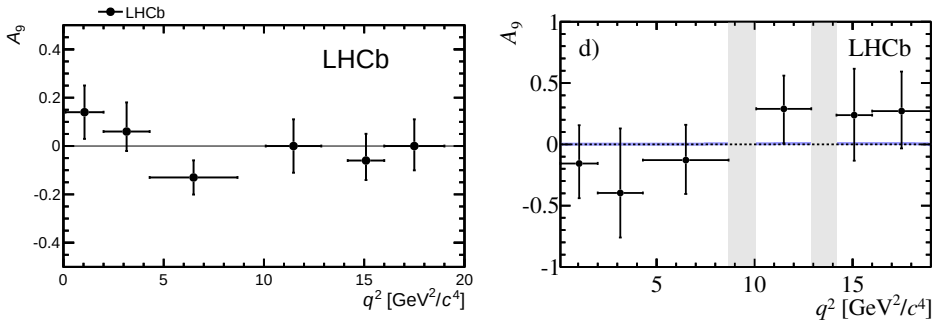

Figure 8: The T-odd asymmetry from the interference of the two transverse amplitudes for the B^0 (left) and B_s^0 (right) decays.

6. Conclusions

We summarized results of the measurement of differential branching fraction as a function of the dimuon invariant mass squared, q^2, in the $B^0 \to K^{*0}\mu^+\mu^-$ and $B_s^0 \to \phi\mu^+\mu^-$ decays. To increase the sensitivity to the photon polarization in $b \to sl^+l^-$ decays, we search for $B^0 \to K^{*0}e^+e^-$ decay at low q^2, where we observe the signal with 4.6σ significance. LHCb has also performed a multidimensional angular analysis of the $B^0 \to K^{*0}\mu^+\mu^-$ decay and a first angular analysis of the $B_s^0 \to \phi\mu^+\mu^-$ decay. These are the world's most precise measurements of the $B^0 \to K^{*0}e^+e^-$, $B^0 \to K^{*0}\mu^+\mu^-$ and $B_s^0 \to \phi\mu^+\mu^-$ decays. Where SM predictions exist, results are consistent with them and place stringent constraints on the contributions from physics beyond SM to $b \to s$ flavour changing neutral current transitions.

References

[1] C. Bobeth, G. Hiller and D. van Dyk, JHEP **07** (2011) 067 [arXiv:1105.0376 [hep-ph]].

[2] M. Beneke, T. Feldmann and D. Seidel, Nucl. Phys. B **612** (2001) 25 [hep-ph/0106067].

[3] B. Grinstein and D. Pirjol, Phys. Rev. D **70** (2004) 114005 [hep-ph/0404250].

[4] M. Beylich, G. Buchalla and T. Feldmann, Eur. Phys. J. C **71** (2011) 1635 [arXiv:1101.5118 [hep-ph]].

[5] P. Ball and R. Zwicky, Phys. Rev. D **71** (2005) 014029 [hep-ph/0412079].

[6] W. Altmannshofer, P. Ball, A. Bharucha, A. J. Buras, D. M. Straub and M. Wick, JHEP **01** (2009) 019 [arXiv:0811.1214 [hep-ph]].

[7] C. Bobeth, G. Hiller and G. Piranishvili, JHEP **07** (2008) 106 [arXiv:0805.2525 [hep-ph]].

[8] R. Aaij *et al.* [LHCb Collaboration], LHCb-PAPER-2013-019, arXiv:1304.6325 [hep-ex].

[9] RAaij *et al.* [LHCb Collaboration], LHCb-PAPER-2013-017, arXiv:1305.2168 [hep-ex].

[10] RAaij *et al.* [LHCb Collaboration], LHCb-PAPER-2013-005, arXiv:1304.3035 [hep-ex].

[11] G. J. Feldman and R. D. Cousins, Phys. Rev. D **57** (1998) 3873 [physics/9711021 [physics.data-an]].

[12] L. Lyons, H. B. Prosper and A. De Roeck, "Statistical issues for LHC physics.", doi:10.5170/CERN-2008-001.